Influence of seabed on very low frequency sound recorded during passage of merchant ships on the New England shelf

D. P. Knobles, Preston S. Wilson, Tracianne B. Neilsen, and William S. Hodgkiss

Citation: The Journal of the Acoustical Society of America **149**, 3294 (2021); doi: 10.1121/10.0004991
View online: https://doi.org/10.1121/10.0004991
View Table of Contents: https://asa.scitation.org/toc/jas/149/5
Published by the Acoustical Society of America

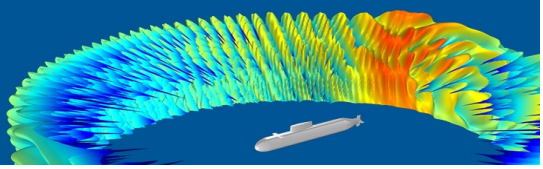

JASA ARTICLE

Influence of seabed on very low frequency sound recorded during passage of merchant ships on the New England shelf

D. P. Knobles,[1,a)] Preston S. Wilson,[2,b)] Tracianne B. Neilsen,[3] and William S. Hodgkiss[4]
[1]*Knobles Scientific and Analysis, Austin, Texas 78731, USA*
[2]*Mechanical Engineering Department and Applied Research Laboratories, The University of Texas at Austin, Austin, Texas 78713, USA*
[3]*Department of Physics and Astronomy, Brigham Young University, Provo, Utah 84602, USA*
[4]*Marine Physical Laboratory and Scripps Institution of Oceanography, University of California, San Diego, La Jolla, California 92093, USA*

ABSTRACT:
An examination of the received spectrogram levels of about twenty merchant ship recordings on two vertical line arrays deployed on the New England continental shelf during the Seabed Characterization Experiment 2017 has identified an acoustic feature that can be attributed to the group velocities of modes 1 and 2 being equal at a frequency $f = \mathcal{F}$. The observation of such a feature is a result of $\beta_{nm}(2\pi\mathcal{F}) = \infty$, where β_{nm} is the waveguide *invariant* for modes n and m. For the New England Mudpatch, the average value of $\mathcal{F}$ is about 24.5 Hz. An effective seabed model is inferred from a feature inversion method that has a deep sediment layer which lies between 190 m and 290 m beneath the seafloor with sound speeds on the order of 1810 m/s. This effective sediment model appears to be consistent with a previous seismic survey on the New England shelf that identified a deep low speed layer about 250 m beneath the water sediment interface. © *2021 Acoustical Society of America*.
https://doi.org/10.1121/10.0004991
(Received 12 February 2021; revised 24 April 2021; accepted 27 April 2021; published online 18 May 2021)
[Editor: Nicholas P. Chotiros] Pages: 3294–3300

I. INTRODUCTION

Since the early 1980s, the acoustic intensity *striations* observed in time-frequency spectrograms have been extensively studied because they contain information about the acoustic propagation in the ocean environment. This information content is useful for both environmental characterization and source localization. In particular, the *waveguide invariant* β has been defined as a quantity that correlates directly to the environment.[1–9] This work identifies a feature in the striation pattern from surface ships over the very low frequency (VLF) portion of the spectrum that may have gone unnoticed in previous studies from shallow water environments with multilayered seabeds. Specifically, this VLF feature is observed on merchant ship spectrograms measured during the 2017 Seabed Characterization Experiment[10] in an area called the New England Mudpatch.[11] Here, we correlate the characteristics of this feature to the geoacoustic structure of a multilayered seabed using a normal mode methodology. Evidence is given that this VLF feature occurs at frequencies where the group velocities of pairs of modes that contribute to a striation become equal, which coincides where $\beta \rightarrow \pm\infty$.

The waveguide invariant has been defined as the slope of the interference striation on a log-log plot of a range-frequency spectrogram. As explained in Ref. 3, by setting a first-order Taylor's series expansion of the acoustic intensity to zero, the waveguide invariant corresponding to the interference between modes m and n is the ratio of the difference in the phase slowness (inverse of the modal phase speed) to the difference in the group slowness (inverse of the model group velocities). This direct dependence on the modal properties of the ocean environment is potentially what makes β a useful tool in environmental characterization of an ocean waveguide.

The remainder of this paper is organized as follows. The feature in ship spectrograms observed on the New England Mudpatch is described in Sec. II. The theoretical formulation that explains the observed feature is discussed in Sec. III. The approach to the inverse problem appears in Sec. IV and Sec. V shows the results of the analyses. The conclusion appears in Sec. VI.

II. OBSERVATION

Ship radiated noise data were recorded on two Marine Physical Laboratory (MPL) Scripps vertical line arrays (VLAs) on the New England continental shelf in 2017.[10] The received level versus frequency and time records were processed for the passage of many merchant ships. About twenty ship passage events possessed an adequate signal to noise ratio to allow direct observation of the VLF feature in the spectrograms. An example is shown in Fig. 1. These low-frequency spectrograms come from the container ship KALAMATA, measured on March 24, 2017 on hydrophone 8 (about 40 m deep) on VLA 1 and VLA 2. Spectrograms

[a)]Electronic mail: dpknobles@kphysics.org
[b)]ORCID: 0000-0002-4420-7180.

 0001-4966/2021/149(5)/3294/7/$30.00

https://doi.org/10.1121/10.0004991

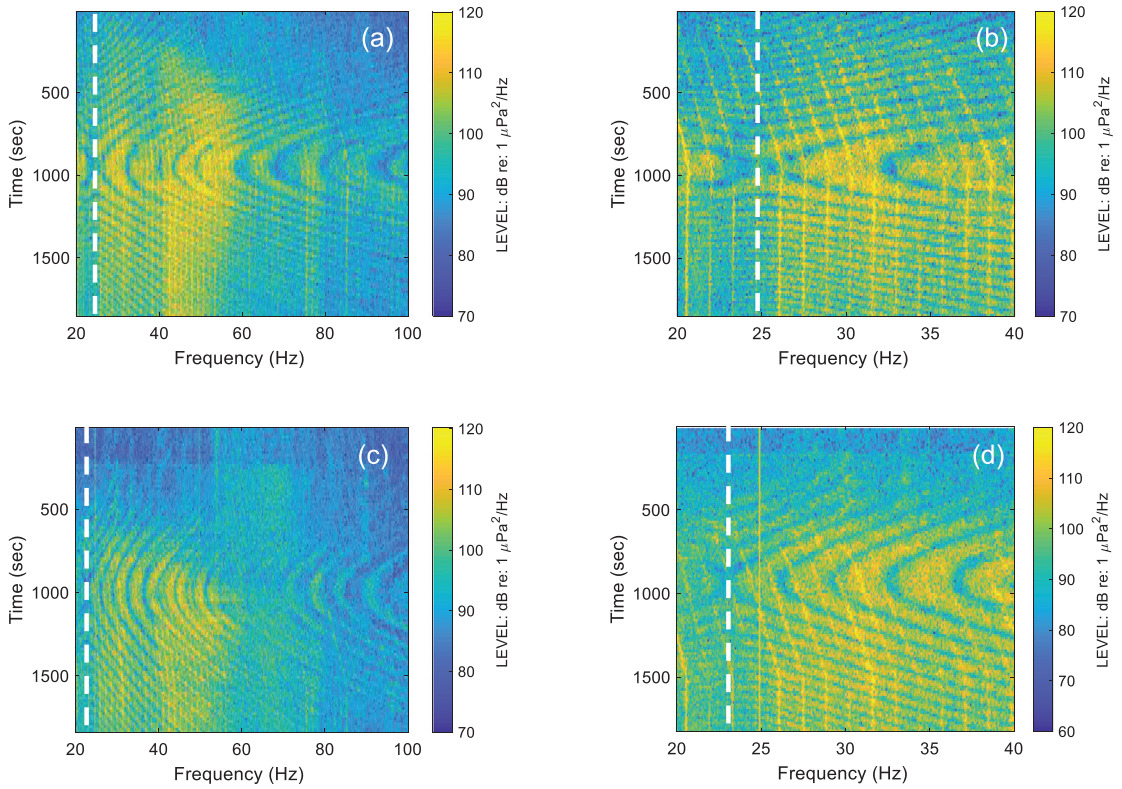

FIG. 1. (Color online) (a) Low-frequency portion of KALAMATA spectrogram measured on VLA 2 in 20–100 Hz band, (b)VLA 2 in 20–40 Hz band, (c) VLA 1 in 20–100 Hz band, (d) VLA 1 in 20–40 Hz band. White dashed lines show the partial axis of symmetry at $f = \mathcal{F}$: approximately 25 Hz for VLA 2 and 23.3 Hz for VLA 1.

are shown for the 20–100 Hz band and the smaller 20–40 Hz band. From automatic identification system (AIS) data, the closest point of approach (CPA) is about 3.3 km and 6.0 km for VLA 2 and VLA 1, respectively, and the ship speed was about 20 kn.

To first order, these spectrograms exhibit a *nested* set of hyperbolas (also known as striations) with the vertices occurring at CPA. The striations are approximately symmetric about the CPA time over a wide frequency band. The symmetry is not exact due in part to a stern/bow aspect dependence of the broadband source level and the fact that the sound propagated upslope to the receivers. In addition to this temporal symmetry, the VLF portion of the spectrograms shows a partial symmetry axis at $f = \mathcal{F}$ (shown by the white dashed line in Fig. 1) that separate two hyperbola branches. The main observation is that the slope of all striations, with respect to frequency, vanishes at $f = \mathcal{F}$. In Sec. 3 it will be shown that $f = \mathcal{F}$ is the frequency where β_{mn} becomes infinite for a mode pair m and n, or equivalently the modal group velocities for modes m and n become equal.

Generally large merchant ships radiate a portion of their sound at discrete frequencies below 50 Hz. One indeed observes in Fig. 1 that superimposed on the broadband striations are a groups of tonals in the 20–40 Hz band. The tonals appear to be associated with the KALAMATA because one observes the same set of tonals as the ship passes both VLA 1 and VLA 2. If a ship is undergoing uniform motion, there will be a Doppler shift to the lower frequencies. However, as the ship passes both CPAs, the tonals have a positive Doppler shift which is consistent with AIS data that had the KALAMATA undergoing a course and speed (increase) change as it approached both VLAs from the east. A detailed analysis of the effect of the motion of the ships on the received spectra is beyond the scope of the present analysis, and no attempt is made to include motion effects or discrete tonals in the acoustic modeling of the spectrograms.

Table I shows the frequencies at which $f = \mathcal{F}$ for twenty merchant ship data samples. $f = \mathcal{F}$ varied from about 22.7 to about 26.2 Hz, with a mean value of 24.5 Hz and a standard deviation of about 1.0 Hz. The observed variability may be ascribed to the variability of the characteristics of the deeper sediment layers in the proximity of the New England Mudpatch. The basis of this statement will be discussed in Sec. VI.

III. FORMULATION

This section presents a physical explanation for why $\beta = \pm\infty$ at $f = \mathcal{F}$. The acoustic pressure in an ocean waveguide can be expressed as a linear response

$$P(z, r) = S(f) * \mathcal{G}, \tag{1}$$

where $\mathcal{G}$ is the complex Green's function solution to the Helmholtz equation for a unit point source and $S(f)$ is the

TABLE I. Observed $\mathcal{F}$ in spectrograms from twenty-one merchant/container ships, along with the closest point of approach (CPA) and ship speed from AIS data.

Data sample	Ship	VLA	$\mathcal{F}$ (Hz)	CPA range (km)	Speed (kn)
1	Hafnia Green	2	25.5	6.2	14.0
2	Atlantic Conveyor	1	26.2	9.0	16.1
3	Maersk Matsuyama	2	25.0	6.2	14.0
4	Maersk Matsuyama	1	22.7	6.2	14.0
5	Viking Bravery	2	25.0	3.1	14.7
6	Viking Bravery	1	25.0	3.3	14.7
7	Atlantic Sea	2	24.0	12.3	17.6
8	Atlantic Sea	1	24.0	9.3	17.6
9	Aniello	2	26.2	3.6	14.3
10	Aniello	1	23.5	6.8	14.3
11	Kalamata	2	25.0	3.2	19.9
12	Kalamata	1	23.4	6.1	19.9
13	Denak Voyager	1	24.5	6.7	10.3
14	Unknown	1	25.0	—	—
15	Corrido	2	24.8	4.0	14.6
16	Corrido	1	24.0	7.0	14.6
17	Corrneille	1	22.5	8.7	17
18	Corrneille	2	25.1	3.7	17
19	YM Unanimity	2	25.0	3.8	9
20	YM Unanimity	1	25.0	6.8	9
21	NYK Diana	1	26.0	8.6	18.9

source function. $\mathcal{G}$ can be expressed as a normal mode expansion

$$\mathcal{G}(f,z_s,z,r)=\frac{i}{4\rho(z_s)}\sum_m \phi_m(z_s)\phi_m(z)H_0^1(k_m r), \tag{2}$$

where k_m and ϕ_m are the horizontal wavenumber eigenvalues and depth dependent eigenfunctions, respectively; r is the source-receiver range; z_s and z are the source and receiver depths, respectively; and $\rho(z_s)$ is the ratio of the density of the fluid medium relative to the density of water at the source depth. When the magnitude of the argument of the Hankel function, $H_0^1(k_m r)$, is greater than 5, its asymptotic approximation can be used and Eq. (2) becomes

$$\mathcal{G}(f,z_s,z,r)=\frac{\sqrt{2\pi}e^{i\pi/4}}{\rho(z_s)}\sum_m \phi_m(z_s)\phi_m(z)\frac{e^{ik_m r}}{\sqrt{k_m r}}. \tag{3}$$

To understand the characteristics of the observed striations in Fig. 1 it is useful to examine the acoustic intensity

$$\mathcal{I}=PP^*=\sum_{mn}|P_{mn}|^2, \tag{4}$$

where $|P_{mn}|^2$ is the acoustic intensity that results from the interaction of two modes m and n:

$$|P_{mn}|^2=|S(f)|^2\frac{1}{r}\left[\frac{A_{mm}}{k_m}+\frac{A_{nn}}{k_n}+2\frac{A_{mn}}{\sqrt{k_n k_m}}\cos(r\Delta k_{mn})\right], \tag{5}$$

where

$$\Delta k_{mn}=k_m-k_n \tag{6}$$

and

$$A_{mn}=\frac{\pi}{8\rho^2(z_z)}\phi_m(z)\phi_m(z_s)\phi_n(z)\phi_n(z_s). \tag{7}$$

From Eq. (5), the range at which modal interference of modes m and n causes a striation is

$$r_{mn}(\ell,\omega)=\frac{2\ell\pi}{\Delta k_{mn}}. \tag{8}$$

Thus, the condition that the slope of a striation vanishes at $f=\mathcal{F}$ is

$$\frac{\partial}{\partial\omega}r_{mn}(\ell,\omega)|_{\omega=2\pi\mathcal{F}}=0 \tag{9}$$

or

$$\frac{\partial}{\partial\omega}\frac{1}{\Delta k_{mn}}|_{\omega=2\pi\mathcal{F}}=0, \tag{10}$$

which is equivalent to

$$-(k_m-k_n)^{-2}\left(\frac{\partial}{\partial\omega}k_m-\frac{\partial}{\partial\omega}k_n\right)=0. \tag{11}$$

For $k_n\neq k_m$ this condition leads to

$$V_m(2\pi\mathcal{F})=V_n(2\pi\mathcal{F}), \tag{12}$$

where the group velocity for mode n is defined as

$$V_n=\left[\frac{\partial}{\partial\omega}k_n(\omega)\right]^{-1}. \tag{13}$$

The waveguide invariant β_{nm} for modes n and m can be defined as[3]

$$\beta_{nm}(\omega)=\frac{\eta_{nm}(\omega)}{\zeta_{nm}(\omega)}, \tag{14}$$

where

$$\eta_{nm}(\omega)=\frac{1}{C_n(\omega)}-\frac{1}{C_m(\omega)}, \tag{15}$$

$$\zeta_{nm}(\omega)=\frac{1}{V_n(\omega)}-\frac{1}{V_m(\omega)}, \tag{16}$$

and the modal phase speed of the nth mode is defined as

$$C_n(\omega)=\frac{\omega}{k_n(\omega)}. \tag{17}$$

Thus, one observes that the condition for the vanishing of the slope of a striation [Eq. (9)] for the non-degenerate case $k_m\neq k_n$ is $\beta=\pm\infty$, which corresponds to $V_m(2\pi\mathcal{F})=V_n(2\pi\mathcal{F})$. Finally, $\beta_{nm}(2\pi\mathcal{F})=+\infty$ for $C_m>C_n$ and $\beta_{nm}(2\pi\mathcal{F})=-\infty$ for $C_m<C_n$.

https://doi.org/10.1121/10.0004991

The VLF feature in the ship spectrograms at $f = \mathcal{F}$ occurs because the group velocities of two modes are the same. Thus, it is necessary to identify the mode pairs that contribute to the observed striation patterns in the frequency band of interest. The need to identify mode pairs is analogous to the need to identify multipath pairs to estimate relative time delays in localization methods such as that reported by Westwood and Knobles.[12] In this study, preliminary simulations of spectrograms (such as those in Fig. 1) with a normal mode model[13,14] showed that modes 1 and 2 were responsible for the striation pattern in the 20–40 Hz band. As the frequency increases, higher-order modes begin to contribute. Thus, an inversion approach based on β_{mn} over a larger bandwidth would need to *a priori* identify multiple pairs of modes that are responsible for the striation patterns. This approach would generally result in a spectrum of $\mathcal{F}$ values. Such an involved study is beyond the scope of the present paper. To clearly understand the cause of the VLF feature showing $\beta = \infty$, we concentrate on the 20–40 Hz band where the striations are dominated by modes 1 and 2.

IV. DEFINITION OF INVERSE PROBLEM

The inversion idea adopted in this study was a matched-feature approach to find optimal values for $\mathcal{F}$. In a feature-based inversion, a solution in parameter space H is found that gives the lowest value for an error function $E(H)$. In this work,

$$E(H) = (\mathcal{F}_{\text{mod}}(H) - \mathcal{F})^2, \tag{18}$$

where $\mathcal{F}_{\text{mod}}(H)$ is the modeled value of the frequency where the group velocities of a selected mode pair become equal.

A critical step of this inversion approach is to select a frequency resolution with which to extract the observed $\mathcal{F}$ value from spectograms. The frequency spacing is determined from a choice of an integration time of $T_{\text{int}} = (1/\Delta f) = 2^N/f_s$, where the sampling rate $f_s = 25$ kHz and N is an integer and T_{int} is much less than the full observation period of the spectrogram. Generally increasing T_{int} provides finer resolution of $\mathcal{F}$. However, a practical limit on T_{int} exists because the ship is moving relative to the receiver, and for each instant of time, the propagation path from the source to the receiver changes. Thus, spatial variability places limitations on the size of T_{int}. In such cases, taken to the extreme too large of T_{int} would *smear* the spectrograms. Fluctuations in the water column that affect the amount of temporal coherence can impose limitations on T_{int}. Fortunately, during SBCEXP, the spatial and temporal variability in the water column were rather small.

The choice of $N = 21$ which gives $T_{\text{int}} \approx 84$ s appeared to be a reasonable choice for the spectrogram data analyzed in this work. This choice gives a frequency resolution of $\Delta f = 0.0119$ Hz and yields 1681 frequency bins in the 20–40 Hz band. Using this Δf, the $\mathcal{F}$ values that were extracted for the spectrogram data samples shown in Fig. 1 for the merchant ship KALAMATA were 24.9982 Hz and 23.3531 Hz for VLA 2 and VLA 1, respectively. For the application of feature inversion we only utilize these values of $\mathcal{F}$ in separate optimizations of selected model geoacoustic parameter values.

The next step of the inversion process was to select a parameter space H. The goal of this work was to understand with the simplest waveguide model possible the physical properties of the seabed that could explain the observed values of $\mathcal{F}$ in the New England Mudpatch. The approach adopted was to create an *effective* horizontally stratified representation of the seabed. For this purpose, a geoacoustic profile was adopted that has four sediment layers over an acoustic basement, as shown in Table II. The model for the first three layers is based in large part on the sub-bottom layering survey and analyses performed by Goff *et al.*[15] The geoacoustic properties in the first layer are based on an analysis by Buckingham,[16] whose grain shearing model provided a good fit to the reported sound speed ratio (inferred and direct measurements from about 15 separate measurements and analyses).[10] The geoacoustic values for the 2 m transition layer followed by another layer of about 7.5 m of sand are based on a transdimensional inversion analyses of reflection data by Belcourt *et al.*[17] The transition layer has a very large sound speed gradient, and has been previously explained by Goff.[15] The total thickness of the mud and transition layer is about 12.3 m, and was established using the two-way travel time bottom layering data from Ref. 15 combined with an analysis of Signal, Underwater Sound (SUS) waveform data.[18] The sound speed in the basement was previously determined independently by Wan[19] and Potty and Miller[20] in modeling broadband data from SUS where the Airy phase frequency for mode 2 was modeled with a basement sound speed of about 1812 m/s. It is of interest to note that the reported Airy phase frequency for mode 2 lies between 26 and 28 Hz which is larger than the observed $\mathcal{F}$. The Airy phase frequency is interpreted as the minimum group velocity for a given mode.

Pre-modeling of the measured striations demonstrated that variations in the sediment structure of the first three layers could not explain the observed $\mathcal{F}$ values. It was hypothesized that the observed value of $\mathcal{F}$ could be ascribed to the existence of a deep fourth layer not reported by Goff.[15] Assuming nominal parameter values for the density and attenuation of this layer, the inversion parameter space

TABLE II. Parameter space for the geoacoustic model used in the inversion. Columns contain layer thickness h (in m) and the sound speed at the top of a layer c_t and at the bottom of a layer c_b (in m/s), the density at the top of a layer ρ_t and at the bottom of a layer ρ_t (in kg/m^3), and attenuation at the top of a layer α_t and at the bottom of a layer α_b (in dB/m-kHz) and the basement.

Layer	h	c_t	c_b	ρ_t	ρ_b	α_t	α_b
1	10.2	1445	1446	1612	1612	0.04	0.04
2	2.0	1446	1710	1.7	1.7	0.15	0.15
3	7.5	1750	1750	1.8	1.8	0.15	0.15
4	[100–300]	[1751–1812]	$c_b = c_t$	2.0	2.0	0.05	0.05
Basement	∞	1812	—	2.2	—	2.2	—

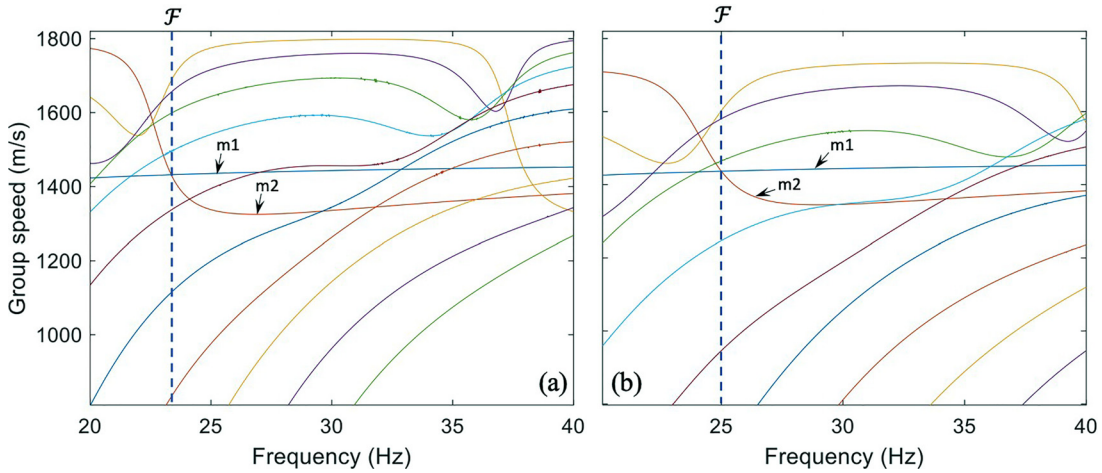

FIG. 2. (Color online) Predicted modal group velocity from optimized geoacoustic profile: (a) VLA 1 and (b) VLA 2. Modes 1 and 2 are labeled "m1" and "m2," respectively. Blue dashed lines indicate $V_1 = V_2$ at $f = \mathcal{F}_{\text{mod}} = \mathcal{F}$.

H, thus, consists of two parameters: the sound speed with upper and a lower bounds of 1751 and 1812 m/s, respectively, and the thickness with a lower and upper bound of 100 and 300 m. The lower and upper bounds of the sediment thickness were determined by a sensitivity study.

The inversion procedure adopted in this study is to use Monte Carlo sampling over the parameter space H. The total number of Monte Carlo samples N_{MC} was selected to be 5000. For each parameter sample, the normal mode eigenvalues $k_n(2\pi\mathbf{f})$ were computed for 1681 frequencies in the 20–40 Hz band for a pre-selected number of modes. The criteria of total mode number selection was made based on the manner in which the ORCA normal mode algorithm finds modes in the complex horizontal wavenumber plane.[13,14]

For each sampling of parameter values in H, $\mathcal{F}_{\text{mod}}$ is found such that $V_m(2\pi\mathcal{F}_{\text{mod}}) = V_n(2\pi\mathcal{F}_{\text{mod}})$, and $\mathcal{F}_{\text{mod}}$ is one of the 1681 processing frequencies in the 20–40 Hz band. Generally, the result of the optimization calculation yields multiple combinations of the sediment thicknesses and the sound speeds that give an error function value $E = 0$. For larger T_{int}, a smaller number of solutions result in $E = 0$. The selection of $T_{\text{int}} \approx 80$ s, which gave 1681 frequencies in the 20–40 Hz band, generally resulted in about 5–10 solutions with $E = 0$. In this work, we report the average value and standard deviations of the sediment thickness and sound speed in the fourth layer for the $E = 0$ solutions.

V. RESULTS

The feature–based inversion scheme was employed with $\mathcal{F} = 24.9982$ Hz and $\mathcal{F} = 23.3531$ Hz for the KALAMATA spectograms measured on VLA 2 and VLA 1, respectively. The optimum sound speeds obtained for the fourth sediment layer were 1810.6 ± 3 m/s and 1753.3 m/s ± 3 m/s for VLA 1 and VLA 2, respectively. The optimum sediment thickness obtained for the fourth sediment layer

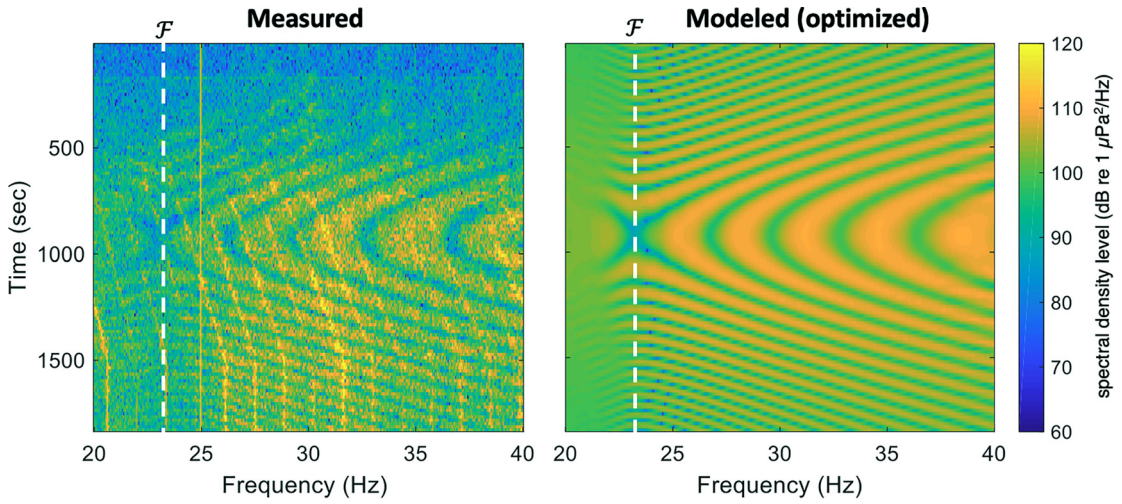

FIG. 3. (Color online) Spectrograms in 20–40 Hz band with $\Delta f = 0.0119$ Hz for KALAMATA of measured and optimized model on VLA 1 with $\mathcal{F} = 23.3531$ Hz indicated by white dashed line. Model spectrogram computed with a CPA range of 6000 m and a source speed of about 20.9 kn and assuming the Wales and Heitmeyer formula for source level (Ref. 21). No attempt was made to include the discrete part of the merchant ship spectrum in the modeled spectrogram.

https://doi.org/10.1121/10.0004991

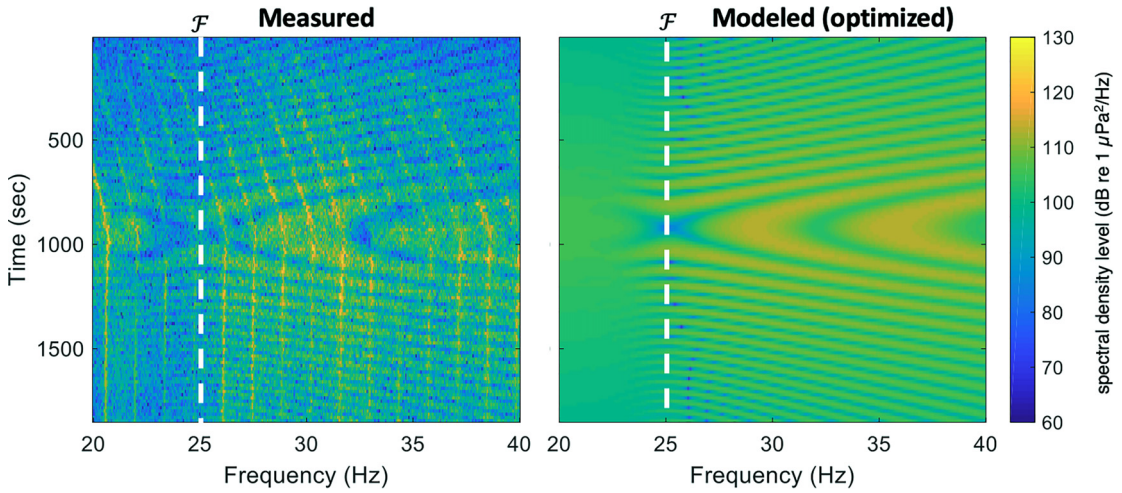

FIG. 4. (Color online) Spectrograms in 20–40 Hz band with $\Delta f = 0.0119$ Hz for KALAMATA of measured and optimized model on VLA 2 with $\mathcal{F} = 24.9982$ Hz indicated by white dashed line. Model spectrogram computed with a CPA range of 3200 m and a source speed of about 20.9 kn and assuming the Wales and Heitmeyer formula for source level (Ref. 21). No attempt was made to include the discrete part of the merchant ship spectrum in the modeled spectrogram.

were $270\,\text{m} \pm 30\,\text{m}$ and $173\,\text{m} \pm 30\,\text{m}$ for VLA 1 and VLA 2, respectively. The uncertainty arises only from the standard deviation of values that produced a value of $E = 0$. If one were to include values of $E > 0$ the uncertainty would increase.

Figure 2 shows the group velocity dispersion curves for the optimized geoacoustic profiles for the VLA 1 and VLA 2 values for $\mathcal{F}$. The group velocity versus frequency was constructed with a five-point numerical derivative[22] of $k_n(2\pi\mathbf{f})$. The critical observation in Fig. 2 is denoted by the blue dashed vertical lines indicating when $V_1(2\pi\mathcal{F}) = V_2(2\pi\mathcal{F})$. Finally, one observes that mode 2 has a broad minimum in its group velocity from about 25–28 Hz, which is consistent with the reporting of the Airy phase frequency in Refs. 18–20 that utilized SUS data to infer seabed properties of the New England Mudpatch.

Figures 3 and 4 compare the optimized model spectrograms to the measured spectrograms for the merchant ship KALAMATA on hydrophone 8 (about 42 m depth) of VLA 1 and VLA 2, respectively. The modeled spectrograms are computed using Eqs. (1) and (2) with the optimized sound speed and sediment thickness in the fourth sediment layer. In the mode sum in Eq. (2), an assumed effective source depth of 8.3 m was used, which is the reported draft of the KALAMATA. The CPA ranges and ship speeds were slightly adjusted to provide a qualitatively good fit between the measured and modeled spectrogram. The adjusted CPA ranges for VLA 1 and VLA 2 were 6000 m and 3250 m, respectively. The adjusted ship speed that was used in the computations was 20.9 kn. The modeled and measured spectrograms are in qualitative agreement.

VI. CONCLUSIONS AND DISCUSSION

Merchant ship spectograms measured on the New England Mudpatch in 2017 revealed a low-frequency feature attributed to the group velocities of modes 1 and 2 being equal at a frequency $\mathcal{F}$. This observations is equivalent to the statement that the waveguide invariant for modes 1 and 2 is infinite at $\mathcal{F}$; i.e., $\beta_{12}(2\pi\mathcal{F}) = +\infty$. The observed average value for $\mathcal{F}$ for about 20 merchant ship data samples was about 24 Hz. The Airy phase frequency for mode 2 is slightly greater than $\mathcal{F}$; the mode 2 group velocity possesses a broad minimum from about 26 to 28 Hz.

It was shown that variations in $\mathcal{F}$ on the order of about 1.5 Hz could be ascribed to changes in the sound speed (50 m/s) and thickness of an effective deep sediment layer. This inferred effective layer appears to be consistent with the results of a seismic survey of the New England shelf performed by Siegel *et al.*[23] in 2014. The seismic study revealed zones of low sediment sound speeds about 250 m below the water sediment interface in an area just east of the Mudpach that extends down to the continental slope. Specifically, Fig. 2 in in Ref. 23 shows a reflector at about 250 m beneath the seafloor and is labeled as a glacial unconformity formed by an ice stream. The two estimates of a deep sediment lie above and below the deepest layer of sediments identified from the survey as overburden pressure. This is consistent with the sound speed only being 1812 m/s. Thus, the existence of a $\beta_{nm}(2\pi\mathcal{F}) = +\infty$ regime may indicate a means for detecting deep sediment properties.

ACKNOWLEDGMENTS

This research was supported by the Office of Naval Research.

[1]S. S. Chuprov, "Interference structure of the sound field in a stratified ocean," in *Ocean Acoustics. Current Status*, edited by L. M. Brekhovskikh (Nauka, Moscow, 1982), pp. 71–91 (in Russian).
[2]G. A. Grachev, "Theory of acoustic field invariants in layered waveguides," Acoust. Phys. **39**, 33–35 (1992).
[3]G. L. D'Spain and W. A. Kuperman, "Application of waveguide invariants to analysis of spectrograms from shallow water environments that vary in range and azimuth," J. Acoust. Soc. Am. **106**, 2454–2468 (1999).

[4]V. M. Kuzkin, "Frequency shifts of the sound field interference pattern in a Shallow Sea," Acoust. Phys. **45**, 224–229 (2002).
[5]C. H. Harrison, "The relation between the waveguide invariant, multipath impulse response, and ray cycles," J. Acoust. Soc. Am. **129**, 2863–2877 (2011).
[6]E. C. Shang, J. R. Wu, and Z. D. Zhao, "Relating waveguide invariant and bottom reflection phase-shift parameter P in a Pekeris waveguide," J. Acoust. Soc. Am. **131**, 3691–3697 (2012).
[7]Y. Le Gall and J. Bonnel, "Passive estimation of the waveguide invariant per pair of modes," J. Acoust. Soc. Am. **134**, EL230–EL236 (2013).
[8]Z. Zhao, J. Wu, and E. Shang, "How the thermocline affects the value of waveguide invariant in shallow water waveguide," J. Acoust. Soc. Am. **138**, 223–231 (2015).
[9]A. H. Young, H. A. Harms, G. W. Hickman, J. S. Rogers, and J. L. Krolik, "Waveguide-invariant-based ranging and receiver localization using tonal sources of opportunity," IEEE J. Ocean Eng. **45**(2), 631–644 (2020).
[10]P. S. Wilson, D. P. Knobles, and T. B. Neilsen, "An overview of Seabed Characterization Experiment," IEEE J. Oceanic Eng. **45**, 1–13 (2020).
[11]D. C. Twichell, C. E. McClennen, and B. Butman, "Morphology and process associated with the accumulation of the fine-grained sediment deposit on the Southern New England Shelf," J. Sediment. Petrol. **51**, 269–280 (1981).
[12]E. K. Westwood and D. P. Knobles, "Source track localization via multipath correlation matching," J. Acoust. Soc. Am. **102**, 2645–2654 (1997).
[13]E. K. Westwood, C. T. Tindle, and N. R. Chapman, "A normal mode model for acoustoelastic ocean environments," J. Acoust. Soc. Am. **100**, 3631–3645 (1996).
[14]E. K. Westwood and R. A. Koch, "Elimination of branch cuts from the normal mode solution using gradient halfspaces," J. Acoust. Soc. Am. **106**, 2513–2523 (1999).
[15]J. A. Goff, J. Chaytor, A. Reed, G. Gawarkiewicz, P. S. Wilson, and D. P. Knobles, "Stratigraphic analysis of a sediment pond within the New England Mud Patch: New constraints from high-resolution chirp acoustic reflection data," Mar. Geol. **412**, 81–94 (2019).
[16]M. J. Buckingham, "Wave speed and attenuation profiles in a stratified marine sediment: Geo-acoustic modeling of seabed layering using the viscous grain shearing theory," J. Acoust. Soc. Am. **148**, 962–974 (2020).
[17]J. Belcourt, C. W. Holland, S. E. Dosso, J. Dettmer, and J. A. Goff, "Depth-dependent geoacoustic inferences with dispersion in the New England MudPatch via reflection coefficient inversion," IEEE J. Ocean. Eng. **45**(1), 69–91 (2020).
[18]D. P. Knobles, P. S. Wilson, J. Goff, L. Wan, M. J. Buckingham, J. D. Chaytor, and M. Badiey, "Maximum entropy derived statistics of sound speed structure in a fine-grained sediment inferred from sparse broadband acoustic measurements on the New England continental shelf," IEEE J. Ocean. Eng. **45**, 161–173 (2020).
[19]L. Wan, M. Badiey, D. P. Knobles, and P. S. Wilson, "The Airy phase of explosive sounds in shallow water," J. Acoust. Soc. Am. **143**, EL199–EL205 (2018).
[20]G. R. Potty and J. H. Miller, "Effect of Shear on Modal Arrival Times," IEEE J. Oceanic Eng. **45**, 103–115 (2020).
[21]S. C. Wales and R. M. Heitmeyer, "An ensemble source spectra model for merchant ship-radiated noise," J. Acoust. Soc. Am. **111**(3), 1211–1231 (2002).
[22]M. Abramowitz and I. A. Stegun, *Handbook of Mathematical Functions with Formulas, Graphs, and Mathematical Tables. National Bureau of Standards Applied Mathematics* (Cambridge University Press, Cambridge, 1972).
[23]J. Siegel, D. Lizarralde, B. Dugan, and M. Person, "Glacially generated overpressure on the New England continental shelf: Integration of full-waveform inversion and overpressure modeling," J. Geophys. Res. **119**, 3393–3409, https://doi.org/10.1002/2013JB010278 (2014).